Article ID: 1000-7032(2024)10-1732-09

A Single-chain Antibody for One-pot Fabrication of Luminescent Gold Nanoclusters and Rabies Virus Imaging in Cells

ZHANG Chunxia[1,2,3], XI Hualong[4], SUN Bo[4], WU Yongge[4], JIANG Chunlai[4], YU Xianghui[4], WU Yuqing[1,2*]

(1. *State Key Laboratory of Supramolecular Structure and Materials, College of Chemistry, Jilin University, Changchun* 130012, *China*;
2. *Institute of Theoretical Chemistry, College of Chemistry, Jilin University, Changchun* 130023, *China*;
3. *Medical Materials Research and Development Center, Tianjin Baogang Rare Earth Research Institute Co., Ltd., Tianjin* 300300, *China*;
4. *National Engineering Laboratory for AIDS Vaccine, School of Life Science, Jilin University, Changchun* 130012, *China*)

* *Corresponding Author, E-mail: yqwu@jlu.edu.cn*

Abstract: The fragile antibody leads to a great challenge as a scaffold to fabricate the luminescent metal nanoclusters using one-pot method. This study presents a stable single-chain anti-body (scFv57R-ATS) for the fabrication of luminescent gold nanoclusters(AuNCs@scFv57R-ATS) and a quick, sensitive rabies virus detection in living cells. In this paper, AuNCs@scFv57R-ATS was designed to specifically recognize antigen RV in modified HeLa cells, which promoted the demonstration of metal nanocluster fluorescent probes for antigen targeting and therapy.

Key words: gold nanoclusters; scFv57R-ATS; rabies virus

CLC number: O482.31 **Document code**: A **DOI**: 10.37188/CJL.20240191

一锅法制备的单链抗体保护荧光金纳米簇及其在细胞成像中的应用

张春霞[1,2,3], 席华龙[4], 孙 博[4], 吴永革[4], 姜春来[4], 于湘晖[4], 吴玉清[1,2*]

(1. 吉林大学化学学院 无机与超分子国家重点实验室, 吉林 长春 130012;
2. 吉林大学化学学院 理论化学研究所, 吉林 长春 130023;
3. 天津包钢稀土研究院有限责任公司 医疗材料研发中心, 天津 300300;
4. 吉林大学生命科学学院 艾滋病疫苗国家工程实验室, 吉林 长春 130012)

摘要: 由于易碎抗体的存在,使得单锅法制备发光金属纳米团簇面临很大挑战。本研究提出了一种稳定的单链抗体(scFv57R-ATS),用于制备发光金纳米团簇(AuNCs@scFv57R-ATS)和在活细胞中快速、敏感地检测狂犬病病毒。本文设计的AuNCs@scFv57R-ATS在被修饰的HeLa细胞中能特异性识别抗原RV,这推动了金属纳米簇荧光探针对于抗原的靶向示踪及治疗示范。

关 键 词: 金纳米簇; scFv57R-ATS; 狂犬病毒

收稿日期: 2024-08-15; **修订日期**: 2024-08-27
基金项目: 国家自然科学基金(1875085,21373101); 吉林省科技发展计划项目(20230204040YY); 吉林大学超分子结构与材料国家重点实验室创新开放项目(sklssm2023017)
Supported by National Natural Science Foundation of China(21875085, 21373101); Jilin Provincial Science and Technology Development Plan Project(20230204040YY); The Innovation & Open Program of the State Key Laboratory of Supramolecular Structure and Materials, Jilin University(sklssm2023017)

1 Introduction

The small metal nanoclusters (MeNCs) generally composed of only decade few atoms often show size-dependent electronic transitions and intense luminescence[1-3]. The discrete electron energy levels resulted in unique properties being highly different from bigger nanoparticles and attracted more researchers' attention recently[4-6]. The gold nanoclusters (AuNCs) fabricated directly by proteins often show good solubility and excellent biocompatibility. Additionally, the active surface groups as —COOH and/or —NH_2 in the protected protein endows it easily to be functionalized as purpose. Several commercially available protein, such as bovine serum albumin (BSA)[7-9], lysozyme[10-11], glucose oxidase (GOx)[12], horseradish peroxidase(HRP)[13], and easily expressed proteins as GST[14] and P53[15] have been successfully used to reduce and stabilize the luminescent AuNCs. However, the harsh conditions as high temperature and extremely basicity used for the fabrication sometimes lead to the partial denaturation and/or biological function lost partially or even entirely of these tolerant proteins[13-15], let alone the more fragile single-chain antibodies. Therefore, regarding of their important role in the immune response of living organisms, antibodies have been rarely used as scaffolds for the one-pot fabrication of luminescent MeNCs. Several approaches to post-conjugate the single-chain antibody to the plasmon gold nanoparticles (AuNPs)[16-20] have been reported, where the performance essentially based on the plasmon absorption rather than the sensitive luminescence. To date, however, there is only one example reported for the one-pot MeNCs synthesis using the anti-BSA IgG directly as a model[21]. It convinced the single-chain antibody a reliable scaffold to reduce and protect luminescent MeNCs.

Besides, reputation as being inevitably fatal, together with its ability to affect all mammalian species, facilitated the fears of rabies over the world. Although post-exposure prophylactic (PEP) by administering rabies vaccine and immunoglobulin (RIG) provided sufficient protection against infection, certain shortcomings limited their use sufficiently. Therefore, genetically engineered antibodies against the rabies virus (RV) came to research recently instead of RIG[22-24]. The single-chain variable antibody fragment (scFv), grafted from the heavy and light chains of immunoglobin, has sprung up recently. Albeit sharing just the smallest unit, the developed scFv possessed both the high binding affinity and specific recognition of the matrilineal antibody[25].

Moreover, the successful expression of the scFv in the prokaryotic system essentially decreased the cost of antibody-producing[26]. For example, the single-chain variable fragment, scFv57R, targeting the glycoprotein of RV was achieved from a clinical mono clone antibody (mAb) of CR57[27]. Besides, the inherent low stability and short half-life *versus* the parent RIG were improved by fusing at the C-terminus an acidic tail of synuclein (ATS) of human alpha-synuclein protein. The ATS labelling on scFv57R, generating a scFv57R-ATS, improved its thermal stability and vastly extended its potential in diagnosis and therapeutics[28].

ATS was proposed to prevent protein aggregation under versatile stresses[29-30]. The inhibition of ATS-fusion on antibody aggregation under extremely pH, high temperature or metal ions was achieved[31]. Moreover, the ATS-tailed antibody showed no apparent decrease on the binding affinity to antigen or neutralizing potency of the original antibody. Remarkably, the obtained scFv57R-ATS showed improved thermal stability and a longer half-life in serum compared to scFv57R. Notably, in the ELISA test, the ATS-fusion vastly improved the protection ability of scFv57R against fatal RV[29-30]. Thus, ATS-fusion is an effective strategy to stabilize antibodies for practical use widely. In the present study, the scFv57R-ATS will be used both as reductant and supported scaffold to directly fabricate the antibody encapsulated AuNCs in one-pot. Thus, a new nanomaterial, possessing both red-emission and immune ability of scFv57R-ATS, was developed. The product, AuNCs@scFv57R-ATS, image the RV-loaded cells brightly and quickly, therefore, supplying a fast

and sensitive luminescence approach for RV detection in cell.

2 Experiment

2.1 Materials

$HAuCl_4 \cdot 3H_2O$, sodium citrate, $Na_2HPO_4 \cdot 12H_2O$, KCl, NaCl, and KH_2PO_4, NaOH were purchased from Beijing Chemical Factory (Beijing, China), with purities higher than 99%. Chemicals obtained from commercial suppliers were used without further purification. Distilled water (ρ =18.2 M·cm, 25 ℃), used for all experiments, was obtained from a water purification system (Millipore Milli-Q).

The recombinant vector of scfv57R-ATS was constructed using the same method as reported[15]. The protein of scFv57R-ATS is composed of the scFv57R and an ATS-tag (DPDNEAYEMPSEEGYQDYEPEA). The expression and purification of the recombinant scFv57R-ATS are also the same as described before[32]. SDS-PAGE analysis, together with the western-blot assay, was used to identify scFv57R-ATS based on a mouse anti-His mAb accordingly.

2.2 Fabrication of the scFv57R-ATS Protected Gold Nanoclusters

We added an aqueous solution of $HAuCl_4$ (10.0 mmol·L^{-1}, 60–130 μL) into a solution of ScFv57-ATS (5.0–20.0 mg·mL^{-1}, 500 μL), respectively, distilled water (340–270 μL) was introduced into the mixture under vigorous stirring. After 10 s, 1.0 mol·L^{-1} NaOH was added to the mixture to adjust the pH from 7.0 to 13.0. After it turned from light yellow to colorless, the solution was quickly heated to the target temperature (40–120 ℃, with an interval of 10 ℃), respectively, and then being kept there for different time (5–60 min) to finalize the reaction. Once the reaction stops, the solution was cooled down and then dialyzed for 24 h using a 10 ku dialysis bag to remove the excess reactants and refold the protein to its natural state as much as possible. The products are stored at 4 ℃ for further characterization and practical use.

2.3 Binding Affinity Assay of scFv57R-ATS and AuNCs@scFv57R-ATS by ELISA

The solution of scFv57R-ATS or AuNCs@scFv57R-ATS in different concentrations (0.002–4.0 mg·mL^{-1}) was added into ELISA plates pre-coated with the inactivated RV ERA strain being blocked. After incubation at 37 ℃ for 1 h, the unbound proteins were washed away with PBST (200 μL, thrice). Then a diluted (1∶1 000) HRP connected anti-His tag antibody (Transking, China) was added (100 μL/well), which reacted at 37 ℃ for 1 h. Again, after washing with PBST (200 μL, thrice), the substrate of tetramethylbenzidine (TMB) was added (100 μL/well), which was incubated at 37 ℃ for another 5 min, protected from light. H_2SO_4 (2 mol·L^{-1}, 50 μL/well) is used to stop the reaction, and the RV binding ability was measured by the absorbance at 490 nm.

2.4 Cell Culture and Fluorescence Images of AuNCs@scFv57R-ATS in RV-free and RV-loaded Living Cells

To study the localization of AuNCs@scFv57R-ATS in cells, particularly the fluorescence response to RV, laser confocal scanning microscopy was adopted to visualize the luminescence image. First, HeLa cells (CCL-2, ATCC) were pre-cultured in a 96-well plate seeded with a density of 1.0×10^5 cells per dish (15.6 mm). Once growing up to a 40% density, RV (MOI=0.01) were loaded in two cell lines while another two free, grown at 37 ℃ under 5% CO_2. After 24 h, followed by removing the medium, 500 μL fresh DMEM with 10% serum medium and AuNCs@scFv57R-ATS or not (final concentration is 1.2 mg·mL^{-1} or 0) was added to each group respectively. Next, the cells were incubated for another 1, 2, 8 h, respectively, at 37 ℃. Subsequently, the cells were washed thrice using the ice-cold PBS (pH 7.4). Finally, we recorded the cell images using an equipment of FV1000 (Olympus, Japan), under the excitation of 490 nm. The staining of DAPI was performed 2–3 min before the measurement, at room temperature.

2.5 Characterizations

A Shimadzu (Japan) RF-5301 fluorescence

spectrophotometer is used to measure luminescence spectra of AuNCs@scFv57R-ATS. UV-Vis absorption spectra measurements were performed on a Shimadzu UV-3600 spectrophotometer using a 1 cm × 1 cm quartz cuvette. X-ray photoelectron spectroscopy (XPS) measurement was performed on an ESCALAB 250 spectrometer with a monochromic X-ray source (Al Kα line, 1486.6 eV). PMS 450 spectropolarimeter (Biologic, France) was used to record the circular dichroism (CD) spectrum. All infrared spectra were characterized by a Vertex 80 V vacuum Fourier transform infrared (FT-IR) spectrometer (Bruker, Germany), where the sample was dispersed in a KBr pellet. The photoluminescence quantum yield (QY) of AuNCs@scFv57-ATS was measured using Quantaurus-QY (Edinburgh Instruments), including an excitation light source composed of a Xe lamp and monochromator. Transmission electron microscopy (TEM) measurements of AuNCs@scFv57R-ATS were conducted with JEM-2200FS (Jeol Ltd, Japan), working with an accelerating voltage of 120 kV. The decay curve of fluorescence emission was measured using FLS920 (Edinburgh Instruments, United Kingdom) *via* combining with a fluorescence lifetime and steady-state spectrometer.

3　Results and Discussion

Under the limitation to vastly improve the protein concentration, initially, different amount of $HAuCl_4$ were added respectively into a solution containing fixed scFv57R-ATS. After heating for 1 h at 60 ℃, the product was purified *via* dialysis, and the corresponding emission spectra were measured (Fig. 1(a)). The increases of $HAuCl_4$ in feeding materials led to bilateral emission changes of product turned between 0.8–0.9 mmol·L^{-1}. Meanwhile, a unilateral blue-shift showed for the product along with $HAuCl_4$ (Fig. 1(a)), indicating a high ratio of protein to $HAuCl_4$ tends to produce red emission as revealed before for GST[14] and p53[15]. The plots in Fig. 1(b) revealed that 0.8 mmol·L^{-1} was the best concentration of $HAuCl_4$ which produced intensive red-emission at 670 nm, albeit less $HAuCl_4$ resulted in higher wavelength but feeble emission.

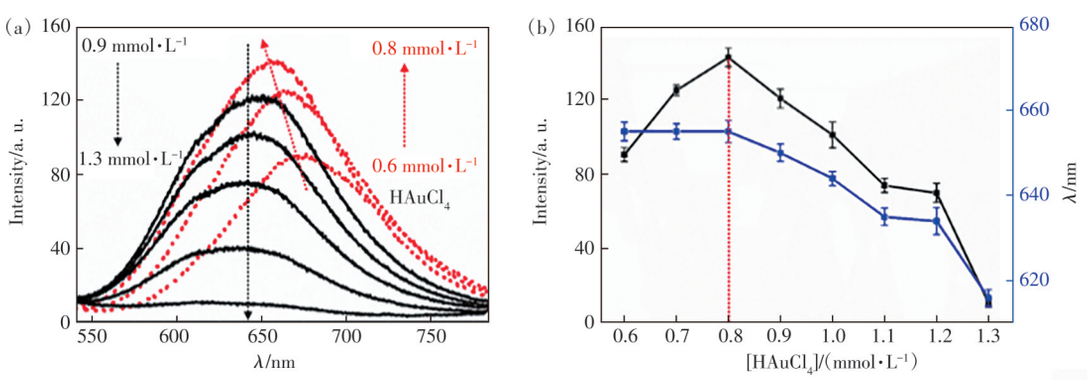

Fig.1　(a) Luminescence spectra of AuNCs@scFv57R-ATS being fabricated at 60 ℃, with different amounts of $HAuCl_4$ between 0.6–0.8 mmol·L^{-1} (red) and 0.9–1.3 mmol·L^{-1} (black), respectively, when scFv57R-ATS is fixed at 10.0 mg·mL^{-1}. (b) Plots of corresponding emission intensity and peak position of (a) (λ_{ex} = 400 nm)

The effects of pH on AuNCs@scFv57R-ATS fabrication were investigated by changing pH from 7.0 to 13.0, respectively, and the emission spectra were recorded (Fig. S1(a)). The requirements for intense and red-emission products resulted in an optimal pH of 12.0 for the fabrication (Fig. S1(b)). Besides, the protein concentration of scFv57R-ATS to produce high-luminescent AuNCs@scFv57-ATS was either optimized (Fig. S1(c)), showing that 20 mg·mL^{-1} is preferred (Fig. S1(d)) for the following synthesis. Finally, we optimized the reaction temperature (Fig. S2) and time (Fig. S3) to improve the optical properties of AuNCs@scFv57-ATS further. As a result, the high luminescence and red-shift products are achieved at 100 ℃; while the most substantial emission ap-pears in 20 min, indicating a

time to stop the reaction enough. In summary, a solution containing fixed amounts of $HAuCl_4$ (0.8 mmol·L^{-1}) and scFv57R-ATS (20.0 mg·mL^{-1}) are chosen to react at 100 ℃ for 20 min, as the best conditions to fabricate the high luminescent, red-emissive AuNCs@scFv57R-ATS in the present study.

The obtained AuNCs@scFv57-ATS emits at 700 nm under the excitation of 590 nm (Fig. 2(a)), which results in a wide Stokes-shift and will benefit its bioapplications. Meanwhile, no absorption peak is shown between 500–700 nm in the spectrum (Fig. 2(b)), excluding giant NPs formation during the fabrication. Also, the TEM image illustrates highly monodisperse metal cores (Fig. 2(c)), most of them locate between 1.35–1.65 nm in size based on a statistic of 200 particles in TEM images (Fig. 2(d)). Compared to the reported AuNCs@GST[14], the distribution of particle size is relatively narrow here.

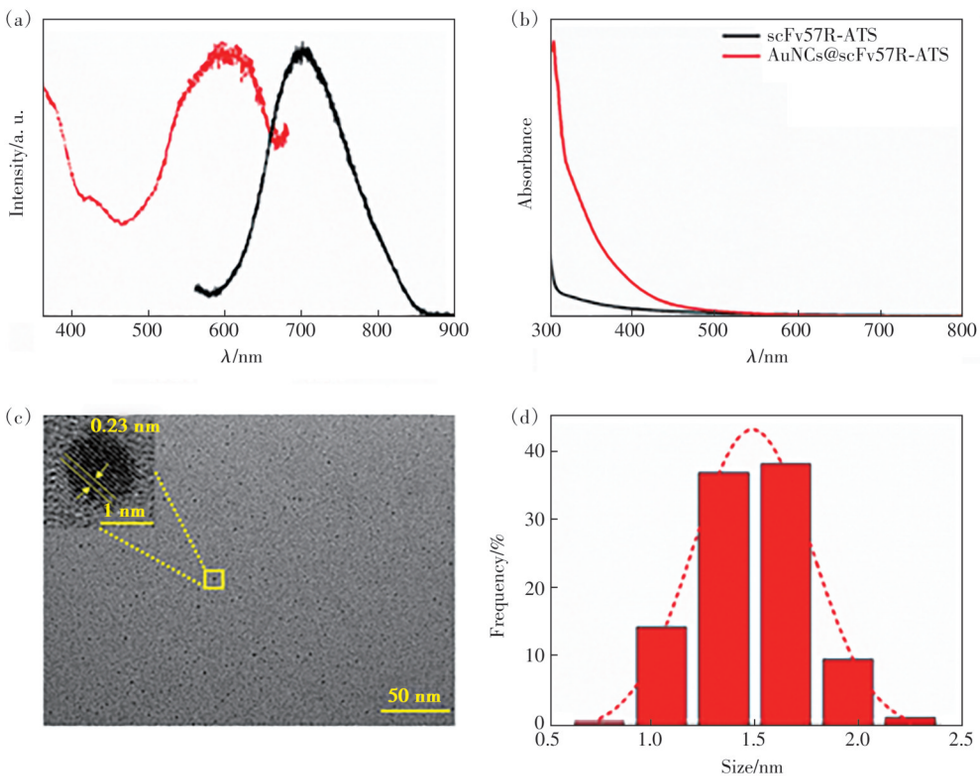

Fig.2 (a) Fluorescence excited (red) and emitted (black) spectrum. (b) UV-visible absorption spectrum of the optimized AuNCs@scFv57R-ATS, respectively. Image of TEM (c) and the distribution of particle size calculated from TEM images (d), inset in (c) is the crystal lattice of the representative particle

We then conducted XPS to investigate the valences of gold in AuNCs@scFv57R-ATS. In Fig. 3(a), the peaks cantered around 84.1 eV and 87.8 eV are assigned to $4f_{7/2}$ and $4f_{5/2}$ of Au[33]. The deconvolution of 84.1 eV into 84.0 eV and 85.0 eV (dot lines) confirms the coexistence of Au(0)/Au(I) in the metal core. The ratio of the integrated areas supplied a content of ~61.4% Au(0) in AuNCs, indicating more than 3/5 gold is presented as Au(0) in the core, whereas the left is present as Au(I) at the surface *via* scFv57R-ATS to stabilize the gold core.

The conformation kept of antibody is crucially necessary to extend the applications of AuNCs@scFv 57R-ATS. We measured infrared (IR) spectra to clarify the antibody structural changes after AuNCs encapsulation. The amide Ⅰ and Ⅱ bands locate between 1 700–1 500 cm^{-1} show no difference between scFv57R-ATS and AuNCs@scFv57R-ATS (Fig. 3(b)), indicating the small size AuNCs inside does not induce an actual conformational change of antibody. Moreover, two negative peaks at 190 nm and 212 nm in the CD spectrum (Fig. 3(c)) indicate the essential β-sheet structure. The high consistency

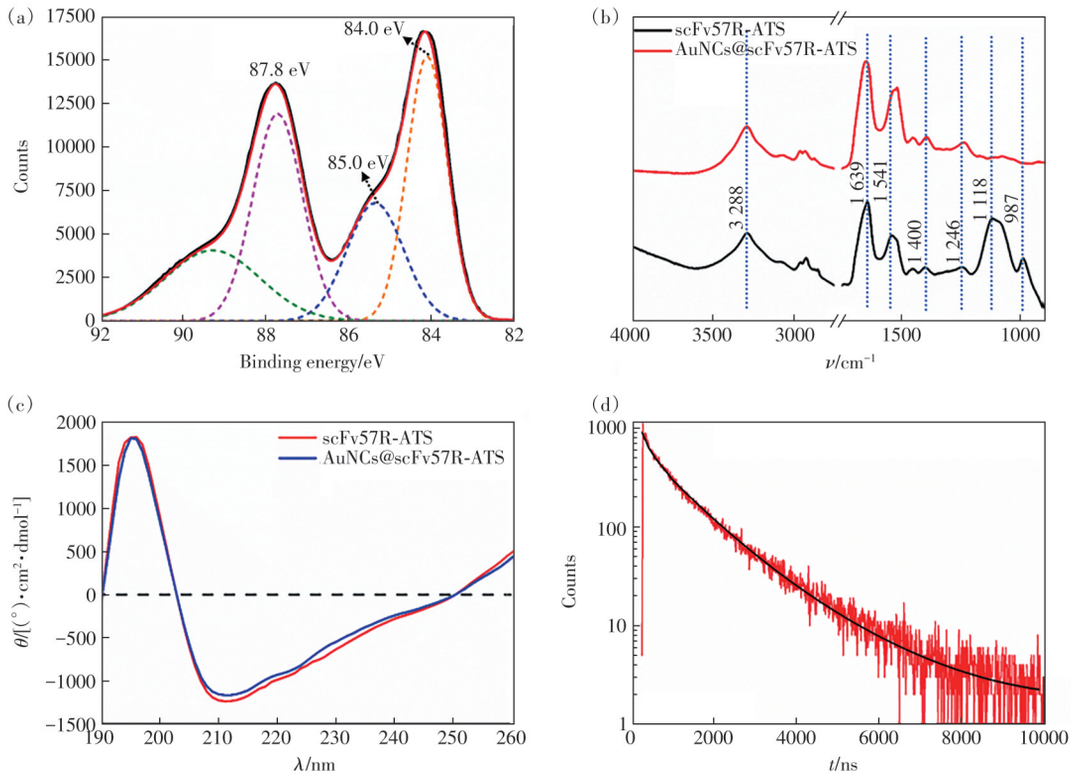

Fig.3　(a) XPS spectra of the optimized AuNCs@scFv57R-ATS. (b) FT-IR spectrum of scFv57R-ATS and AuNCs@scFv57R-ATS in KBr pellet. (c) CD spectra in PBS solution (20 mg·mL^{-1}), respectively. (d) Time-resolved luminescence decay curve of AuNCs@scFv57R-ATS in PBS solution (20 mg·mL^{-1})

between it and that of AuNCs@scFv57R-ATS confirms the intact structure of scFv57R-ATS after AuNCs encapsulation. Combining FT-IR and CD spectra concludes that scFv57R-ATS maintained its structure well after embedding AuNCs inside, which is significant for keeping the biofunctions and binding affinity of the achieved nanomaterial to RV.

We then measured the time-resolved emission decay curve of AuNCs@scFv57R-ATS (Fig. 3(d)) and evaluated the corresponding parameters accordingly. A sole lifetime of τ_1 = 1.009 μs (100%) is revealed based on the curve-fitting (χ^2 = 1.174). Compared to the AuNCs@GST[14] and AuNCs@BSA[34] achieved before, this value is close but unique, indicating the homogeneity of metal core in products. The quantum yield (QY) of the AuNCs@scFv57R-ATS was test based on a standard method[14-15], which offers a value of 1.06% for the optimized AuNCs@scFv57R-ATS in PBS buffer. Such a deal is not high, even among the red-emission metal NCs[14,34]. However, the ATS-fusion paved the way by developing fragile antibodies as a scaffold to fabricate luminescent metallic NCs.

The stability of AuNCs@scFv57R-ATS was assayed (Fig. S4(a)), its emission intensity maintained almost the same as initial value after keeping in dark for three months (4 ℃). Besides, the time-dependent fluorescence spectra were test at 4, 25, 37, 50, 60 ℃, respectively, confirmed the excellent thermal stability (Fig. S4 (b), (c)) as that of AuNCs@BSA[34] at identical conditions. Therefore, the AuNCs@scFv57R-ATS has high stability as AuNCs@BSA in water, which is vital to extend it to luminescence tests and images in living cells.

An indirect ELISA[28] was used to evaluate the binding affinity of AuNCs@scFv57R-ATS to RV. Because of a His-tag containing in scFv57R-ATS, the ScFvs that had already bind to RV were measured using an anti-His mAb from mouse which was further validated by the HRP-conjugated rabbit anti-mouse IgG. As a result, the binding ability of AuNCs@scFv57R-ATS to RV was revealed significantly weaker in

comparison to that of scFv57R-ATS itself but was very close to that of negative control (Data not shown). Such value may be attributed to the occupation of His-tag in AuNCs@scFv57R-ATS through strong binding of histidine to the metal surface[35-36], which consequently lost the binding ability to the mAb of anti-His.

To further confirm it, a novel ELISA by utilizing RVG179 after biotinylation[37] was then performed. RVG179 is a truncated G protein (residues 179–281) derived from the ERA strain of RV, which contained the binding epitope and is often used to evaluate the binding ability of the antibody to RV instead of the intact RV particle. Therefore, the binding abilities of AuNCs@scFv57R-ATS and scFv57R-ATS to RV were evaluated through the novel ELISA by utilizing the biotin-labelled RV179 and HRP-conjugated streptavidin (Fig. S5(a)). The binding ability of AuNCs@scFv57R-ATS to RV (Fig. S5(b)) was nearly identical to that of scFv57R-ATS itself according to the recorded OD_{450}, confirming the intact function of the antibody after AuNCs encapsulation. Besides, the binding affinity difference between novel ELISA and anti-His mAb indeed indicated the blocking of His-tag in AuNCs@scFv57R-ATS, possibly together with other binding sites in ATS and/or ScFv to the metal core.

The AuNCs@scFv57R-ATS was then applied to perform the fluorescence image in living cells. The clearly shown Hela cells, in the control groups without the participation of AuNCs@scFv57R-ATS (Fig. 4(a), (b)), valid the good growth of them after RV-loading and DAPI staining. The merging of them (Fig. 4(c)) indicates that DAPI is genuinely located in the cells' nucleus accordingly[38]. Besides, without DAPI staining and AuNCs@scFv57R-ATS, only a dark field is shown for the blank (Fig. 4(d)). However, for the RV-loaded Hela cells, in the presence of 5 (Fig. 4(e)) or 10 mg·mL^{-1} (Fig. 4(f)) AuNCs@scFv57R-ATS in medium, 30 min incubation lead bright-red color in cells under the 490 nm irradiation. The exact amount of AuNCs@scFv57R-ATS was either added for RV-free cells in parallel. After incubation for 2 h or even 8 h, almost no color was shown for the test group (Fig. S6). Therefore, it suggests that the quick entry of AuNCs@scFv57R-ATS to the RV-loaded cells essentially attributes to the highly specific recognition of scFv57R-ATS to RV, which pushes the probe entry will be used for the fast RV detection in live cells[39].

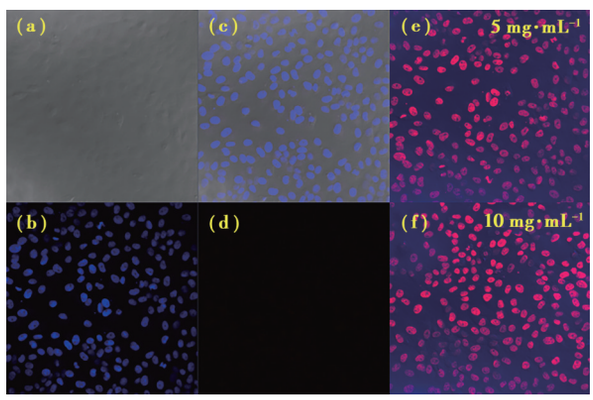

Fig.4 Cell images of the RV-loaded HeLa cells without ((a)–(d)) and with AuNC@scFv57R-ATS((e)–(f)). (a)–(d) The control groups, no AuNCs present during incubation except PBS solution: (a) under white-light, (b) after DAPI staining, (c) image merging of (a) plus (b), (d) dark field. (e)–(f) The RV-loaded Hela cells with 5 mg·mL^{-1} (e) and 10 mg·mL^{-1} (f) AuNCs@scFv57R-ATS, respectively, after 30 min incubation(λ_{ex} = 490 nm)

4 Conclusion

In summary, based on a well-designed single-chain antibody, a novel gold nanocluster, AuNCs@scFv57R-ATS, was successfully fabricated using the one-pot approach. The characterizations by XPS, TEM, FT-IR, and CD spectra confirmed the intact structure of scFv57R-ATS after AuNCs encapsulation. Remarkably, the keeping of anti-body property in ligand was used for the fluorescence image of RV-loaded cells and further the quick and sensitive RV detection in living cells. Therefore, a direct fluorescence approach for RV detection in cells was established. Furthermore, both the design concept and the synthetic approach can be applied to the synthesis of metal nanoclusters using other species of fragile antibodies after improvement.

Supplementary Information and Response Letter are available for this paper at: http://cjl. lightpublishing. cn/thesisDetails#10. 37188/CJL. 20240191.

References:

[1] ZHENG J, ZHANG C W, DICKSON R M. Highly fluorescent, water-soluble, size-tunable gold quantum dots [J]. *Phys. Rev. Lett.*, 2004, 93(7): 077402.

[2] WEI W T, LU Y Z, CHEN W, *et al.* One-pot synthesis, photoluminescence, and electrocatalytic properties of subnanometer-sized copper clusters [J]. *J. Am. Chem. Soc.*, 2011, 133(7): 2060-2063.

[3] TANAKA S I, MIYAZAKI J, TIWARI D K, *et al.* Fluorescent platinum nanoclusters: synthesis, purification, characterization, and application to bioimaging [J]. *Angew. Chem. Int. Ed.*, 2011, 50(2): 431-435.

[4] CHENG D J, LIU R, HU K. Gold nanoclusters: photophysical properties and photocatalytic applications [J]. *Front. Chem.*, 2022, 10: 958626.

[5] MAITY S, KOLAY S, GHOSH S, *et al.* Unraveling the effect of single atom doping on the carrier relaxation dynamics of MAg_{24}^{n-} nanoclusters [J]. *J. Phys. Chem. Lett.*, 2022, 13(24): 5581-5588.

[6] DU Y X, LI C Q, DAI Y L, *et al.* Recent progress in atomically precise metal nanoclusters for photocatalytic application [J]. *Nanoscale Horiz.*, 2024, 9(8): 1262-1278.

[7] ICHIMARU H, HANAZAWA N, ORITA E, *et al.* Preparation of hydrophobic bovine-serum-albumin-capped gold nanoclusters and encapsulation in polystyrene nanoparticles [J]. *e-J. Surf. Sci. Nanotec.*, 2024, 22(2): 115-119.

[8] LU Y T, GUO Y, LIANG X, *et al.* The recognition of aristolochic acid I based on fluorescence quenching of bovine serum albumin-stabilized gold nanoclusters [J]. *Anal. Methods*, 2022, 14(20): 1963-1972.

[9] ZHANG X Y, HUANG Z Z, ZHANG L, *et al.* Synthesis of Au nanoclusters by reduction of bovine serum albumin: the role of sodium hydroxide [J]. *Langmuir*, 2023, 39(19): 6748-6755.

[10] DENG Y L, GUO Y, ZHANG Y D. Aggregation of gold nanoclusters in amyloid fibers: a luminescence assay for amyloid fibrillation detection and inhibitor screening [J]. *Analyst*, 2024, 149(3): 870-875.

[11] CHUANG C H, CHEN W Y, TSENG W B, *et al.* Microwave-mediated synthesis of near-infrared-emitting silver ion-modified gold nanoclusters for ratiometric sensing of hydrosulfide in environmental water and hydrogen sulfide in live cells [J]. *ACS Sustainable Chem. Eng.*, 2022, 10(7): 2461-2472.

[12] 欧丽娟, 李京, 张超群, 等. 氧化反应调控的金纳米簇“关-开”型荧光探针检测过氧化氢和葡萄糖 [J]. 光谱学与光谱分析, 2022, 42(12): 3757-3761.
OU L J, LI J, ZHANG C Q, *et al.* Redox-controlled turn-on fluorescence sensor for H_2O_2 and glucose using DNA-template gold nanoclusters [J]. *Spectrosc. Spect. Anal.*, 2022, 42(12): 3757-3761. (in Chinese)

[13] XIA X H, DUOLIHONG B, MA X D, *et al.* Peroxidase-modified Au@sulfur-doped graphene was constructed for the electrochemical determination of trans-resveratrol [J]. *J. Solid State. Electr.*, 2024, 28(8): 2669-2677.

[14] FU D Y, XUE Y R, GUO Y Q, *et al.* Strong red-emitting gold nanoclusters protected by glutathione *S*-transferase [J]. *Nanoscale*, 2018, 10(48): 23141-23148.

[15] YUAN X X, JIA X Y, LI H W, *et al.* Red-emitting p53-protected gold nanoclusters and their screening of anti-tumor agents from Chinese medicine [J]. *RSC Adv.*, 2017, 7(54): 34276-34282.

[16] GANDHI S, BANGA I, MAURYA P K, *et al.* A gold nanoparticle-single-chain fragment variable antibody as an immunoprobe for rapid detection of morphine by dipstick [J]. *RSC Adv.*, 2018, 8(3): 1511-1518.

[17] LIU Y, LIU Y, MERNAUGH R L, *et al.* Single chain fragment variable recombinant antibody functionalized gold nanoparticles for a highly sensitive colorimetric immunoassay [J]. *Biosens. Bioelectron.*, 2009, 24(9): 2853-2857.

[18] ACKERSON C J, JADZINSKY P D, JENSEN G J, *et al.* Rigid, specific, and discrete gold nanoparticle/antibody conjugates [J]. *J. Am. Chem. Soc.*, 2006, 128(8): 2635-2640.

[19] BYUN J Y, SHIN Y B, LI T H, *et al.* The use of an engineered single chain variable fragment in a localized surface plasmon resonance method for analysis of the C-reactive protein [J]. *Chem. Commun.*, 2013, 49(82): 9497-9499.

[20] PHAM V D, HOANG H, PHAN T H, *et al.* Production of antibody labeled gold nanoparticles for influenza virus H5N1 diagnosis kit development [J]. *Adv. Nat. Sci.: Nanosci. Nanotechnol.*, 2012, 3(4): 045017.

[21] MORA-SANZ V, SAA L, BRIZ N, *et al.* Antibody-directed synthesis of catalytic nanoclusters for bioanalytical assays [J]. *ACS Appl. Mater. Inter.*, 2020, 12(26): 28993-28999.

[22] LEE J H, PARK D Y, LEE K J, *et al.* Intracellular reprogramming of expression, glycosylation, and function of a plant-derived antiviral therapeutic monoclonal antibody [J]. *PLoS One*, 2013, 8(8): e68772.

[23] BOTH L, VAN DOLLEWEERD C, WRIGHT E, *et al*. Production, characterization, and antigen specificity of recombinant 62-71-3, a candidate monoclonal antibody for rabies prophylaxis in humans [J]. *FASEB J.*, 2013, 27(5): 2055-2065.

[24] VAN DOLLEWEERD C J, TEH A Y H, BANYARD A C, *et al*. Engineering, expression in transgenic plants and characterisation of E559, a rabies virus-neutralising monoclonal antibody [J]. *J. Infect. Dis.*, 2014, 210(2): 200-208.

[25] BAKKER A B H, PYTHON C, KISSLING C J, *et al*. First administration to humans of a monoclonal antibody cocktail against rabies virus: safety, tolerability, and neutralizing activity [J]. *Vaccine*, 2008, 26(47): 5922-5927.

[26] HUMPHREYS D P, GLOVER D J. Therapeutic antibody production technologies: molecules, applications, expression and purification [J]. *Curr. Opin. Drug Discov. Devel.*, 2001, 4(2): 172-185.

[27] CHENG Y, LI Z, XI H L, *et al*. A VL-linker-VH orientation dependent single chain variable antibody fragment against rabies virus g protein with enhanced neutralizing potency *in vivo* [J]. *Protein Pept. Lett.*, 2016, 23(1): 24-32.

[28] XI H L, ZHANG K X, YIN Y C, *et al*. Fusion peptide improves stability and bioactivity of single chain antibody against rabies virus [J]. *J. Microbiol. Biotechnol.*, 2017, 27(4): 718-724.

[29] PARK S M, AHN K J, JUNG H Y, *et al*. Effects of novel peptides derived from the acidic tail of synuclein (ATS) on the aggregation and stability of fusion proteins [J]. *Protein Eng. Des. Sel.*, 2004, 17(3): 251-260.

[30] LEE E N, KIM Y M, LEE H J, *et al*. Stabilizing peptide fusion for solving the stability and solubility problems of therapeutic proteins [J]. *Pharm. Res.*, 2005, 22(10): 1735-1746.

[31] GOLDMAN E R, BROZOZOG-LEE P A, ZABETAKIS D, *et al*. Negative tail fusions can improve ruggedness of single domain antibodies [J]. *Protein Expr. Purif.*, 2014, 95: 226-232.

[32] YUAN R S, CHEN X X, CHEN Y, *et al*. Preparation and diagnostic use of a novel recombinant single-chain antibody against rabies virus glycoprotein [J]. *Appl. Microbiol. Biotechnol.*, 2014, 98(4): 1547-1555.

[33] LIU J, LI H W, WANG W X, *et al*. Thermally prepared ultrabright adenosine monophosphate capped gold nanoclusters and the intrinsic mechanism [J]. *J. Mater. Chem.* B, 2017, 5(19): 3550-3556.

[34] YUE Y, LIU T Y, LI H W, *et al*. Microwave-assisted synthesis of BSA-protected small gold nanoclusters and their fluorescence-enhanced sensing of silver(I) ions [J]. *Nanoscale*, 2012, 4(7): 2251-2254.

[35] BUDURU P, REDDY B C S R, NAIDU N V S. Functionalization of silver nanoparticles with glutamine and histidine for simple and selective detection of Hg^{2+} ion in water samples [J]. *Sens. Actuators* B: *Chem.*, 2017, 244: 972-982.

[36] CHU Y Z, KHAN M A, XIA M Z, *et al*. Synthesis and micro-mechanistic studies of histidine modified montmorillonite for lead(II) and copper(II) adsorption from wastewater [J]. *Chem. Eng. Res. Des.*, 2020, 157: 142-152.

[37] DUAN Y, GU T J, JIANG C L, *et al*. A novel disulfide-stabilized single-chain variable antibody fragment against rabies virus G protein with enhanced *in vivo* neutralizing potency [J]. *Mol. Immunol.*, 2012, 51(2): 188-196.

[38] TERASHIMA M, KAMAGATA Y, KATO S. Rapid enrichment and isolation of polyphosphate-accumulating organisms through 4'6-Diamidino-2-Phenylindole (DAPI) staining with fluorescence-activated cell sorting (FACS) [J]. *Front. Microbiol.*, 2020, 11: 793.

[39] 王俊, 张兵波. 纳米长余辉发光材料在生物医学检测、生物成像与肿瘤治疗中的研究进展 [J]. 发光学报, 2024, 45(2): 252-268.
WANG J, ZHANG B B. Research progress of persistent luminescent nanoparticles in biomedical detection, bioimaging and tumor therapy [J]. *Chin. J. Lumin.*, 2024, 45(2): 252-268. (in Chinese)

张春霞(1993-),女,河北盐山县人,博士,高级工程师,2022年于吉林大学获得博士学位,主要从事稀土金属纳米簇的合成与医用新材料的研究。
E-mail: xtzcx@brire.com

吴玉清(1966-),女,吉林长春人,博士,教授,博士生导师,1998年于吉林大学获得博士学位,主要从事纳米生物技术及方法学的研究。
E-mail: yqwu@jlu.edu.cn